Thin-Walled Structures 190 (2023) 111014

Contents lists available at ScienceDirect

Thin-Walled Structures

journal homepage: www.elsevier.com/locate/tws

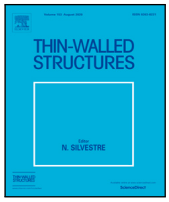

Full length article

Tensile behaviour of asymmetric bolted square hollow section column splices

Rui Yan [a,*], Haohui Xin [b], Milan Veljkovic [a], Luís Simões Da Silva [c]

[a] Department of Engineering Structures, Delft University of Technology, Delft, The Netherlands
[b] School of Human Settlements and Civil Engineering, Xi'an Jiaotong University, Xi'an, China
[c] Department of Civil Engineering, University of Coimbra, Coimbra, Portugal

ARTICLE INFO

Keywords:
Asymmetric column splices
Bolted connection
Component method
Yield line
Square hollow section

ABSTRACT

In traditional end plate column splices, bolts are placed double symmetrically on the four sides of square hollow sections (SHS). In order to reduce the required gap between the façade and the column, the end plate could be flushed on one or two sides of SHS for the column along the façade or at the corner of a building, respectively. However, the analytical solution (Component method) for the traditional column splice is not applicable in this case. This paper addresses the tensile behaviour of asymmetric column splices, where a cover plate is used on the end plate flushed side. Columns are dominantly loaded in compression and bending, but to verify the component's interaction, the column splices are tested in tension in this paper. The tensile behaviour is investigated through the experiment, the finite element (FE) analysis, and the component method. Eight tensile tests were conducted. The FE model is validated against the experiment. A bi-linear model is employed to characterise the column splice yield resistance, which shows a good agreement with the ultimate resistance of the FE model using a constitutive model without strain hardening. The effective length measured from the FE model is approximately two times that calculated by equations. Using the measured effective length, the component method predicts the characterised yield resistance well (average 13% lower). In comparison, the resistance is underestimated by 35% on average if the calculated effective length is used.

1. Introduction

Tubular columns are commonly used in off-site prefabricated structures due to the light self-weight, visually attractive shape, excellent torsion resistance and close equivalent stiffness in two main directions. Fast executions require easy connections. In recent years, many innovative bolted tubular joints connected by different bolts have been proposed and investigated [1–8]. Blind bolts and hollo bolts, suitable for tightening from one side only, are used for connecting the tubular column splices [1] and open section beams to tubular column joints [2, 3]. He et al. [4] tested a blind-bolted T-stub with end plate tapping. The new connection is applicable to the prefabricated joint of open section beams and tubular columns with threads on the inner wall of a screw hole. Alternatively, long bolts connection is becoming very common in practice, such as tubular joints with gusset plates [5], column splices [6], and an innovative beam-to-hybrid fabricated column joint [8].

A traditional solution for tubular column splices is to pre-weld an end plate to the end of the hollow section in the factory and bolt two end plates on the construction site. prEN1993-1-8 [9] prescribes design rules (component method) for the bolted end plate joint with open cross-section members. However, design rules are not available for bolted tubular column splices. Therefore, it is necessary to develop the component method for tubular column splices to facilitate the application. Note that prEN1993-1-8 is a temporary name for the new version of EN1993-1-8, which is under revision. It will be called EN1993-1-8 hereafter.

Extensive tensile tests have been conducted on traditional bolted square hollow section (SHS) and rectangular hollow section (RHS) column splices since the 1980s. Bolts on four sides [10–12] and two sides [12–14] of the hollow section have been investigated. A two-dimensional yield line model was proposed for SHS column splices by Kato and Mukai [10], as shown in Fig. 1. The red dashed line represents the yield line. Packer et al. [13] proposed a one-dimensional design model with six failure modes for RHS two-sided bolted column splices within the framework proposed by Struik and De Back [15]. The six failure modes are depicted in Fig. 2. Failure modes 1 and 2 are the failure of the bolt and column, respectively. Failure modes 3–6 are the yielding of the end plate. The black point represents the plastic hinge in the end plate. The plastic hinge close to the column faces may appear at two possible locations in the end plate. One possible location is along the outside periphery of the weld line, as presented in failure modes 3 and 5. Another is inside the tube, as presented in failure modes 4 and 6. Karlsen and Aalberg [12] found that the T-stub model in prEN1993-1-8 [9] could be used to predict the resistance

* Corresponding author.
E-mail address: r.yan@tudelft.nl (R. Yan).

https://doi.org/10.1016/j.tws.2023.111014
Received 21 November 2022; Received in revised form 24 May 2023; Accepted 8 July 2023
Available online xxxx

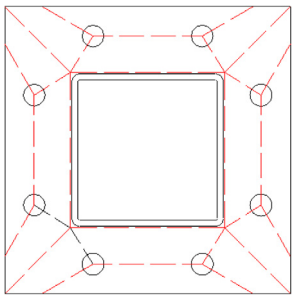

Fig. 1. Two-dimensional yield line model [10].

of the column splice provided bolts symmetrically positioned on two opposite sides. Based on a two-dimensional yield line model developed by Willibald [11], Steige and Weynand [16] proposed an equation, also suggested by CIDECT [17], to estimate the effective yield line length at the corner of the end plate. The equation was simplified by Couchaux et al. [18], obtaining an accurate prediction of the resistance. Based on experimental results in the literature [19,20], Heinisuo et al. [21] proposed three failure modes (see Fig. 3) for the configuration with bolts symmetrically placed at the corner. The red dashed line represents the yield line in the end plate. Ding et al. [22] investigated the effect of the stiffener on the tensile behaviour of the bolted end plate column splices. Six connections with different stiffener configurations were tested experimentally and numerically. It was found that the stiffener may increase the resistance and stiffness significantly if the stiffener were positioned at the corner of the tube.

The traditional column splices are not suitable to position next to the façade, as the end plate needs to be flushed to allow for the easy attachment of the façade panels. In recent years, researchers have explored various innovative configurations to avoid this problem [1,23–28]. Li et al. [1] investigated the moment resistance of a blind-bolted SHS column splice by using an inner sleeve to connect two columns and avoiding the use of sticking-out end plates. A revised yield line model was proposed to predict the static moment resistance of the column splice. Given the importance of the seismic behaviour for modular buildings, other researchers also examined the beam-to-column joints with column splices connected by an inner sleeve [25,27]. Sendanayake et al. [23] proposed two innovative inter-modular connections for SHS column splices. To account for the attached exterior façade or wall, the end plate was flushed on the corresponding side, which was also done in [25,27]. However, since the end plate flushed sides do not have an effective connection, the joint cannot resist the bending moment with end plate flushed side in tension. Hence, two new configurations of asymmetric bolted SHS column splices, as shown in Fig. 4, are proposed in this paper. The advantage of the asymmetric column splice is that no space is required between the façade panel and the column whilst the easy assembly feature remains. It is worth mentioning that columns are dominantly loaded in compression and bending, but for the sake of verifying the component's interaction, the tensile behaviour of the column splice is investigated. Since the component method is not available for bolted hollow section joints in EN1993-1-8, the present work would contribute to the design rules by extending the applicable range to asymmetric SHS joints.

2. Experimental program and finite element (FE) model

2.1. Geometry of specimens

A cover plate is used on the SHS side, where the end plate is flushed to the profile. Fig. 4 depicts the two column splice configurations:

- "Corner" column splice with two cover plates;
- " Wall" column splice with one cover plate.

Table 1
Measured thickness [mm].

Specimen	Hollow section	End plate	Cover plate	Welds (Throat)
WCS-6-A	7.7	6.0	6.0	9.3
WCS-6-B		6.0	6.0	8.7
WCS-8-A		8.5	7.9	8.8
WCS-8-B		8.5	7.9	8.9
CCS-6-A		6.0	6.0	9.1
CCS-6-B		6.0	6.0	8.4
CCS-8-A		8.5	7.9	9.5
CCS-8-B		8.5	7.9	8.7

Each specimen consists of cold-formed SHS tubes, end plates, cover plates, M24 bolts, and M20 bolts. The steel grade of the steel plate and the hollow section is S355. The nominal dimension of the SHS tube is 200 × 200 × 8. The cover plate and endplate were cut from the same plate. The end plate was welded to the end of the column with a nominally 9 mm fillet weld (the thick black line in Appendix A). The cover plate was welded to SHS1 and bolted to SHS2 using M20 bolts. The fillet weld was applied on three sides of the cover plate, represented by the thick black line in Appendix B. The throat thickness of the fillet weld on the end plate was measured at different locations in the specimens. The average throat thickness of the weld, and the measured thickness of the end plate, cover plate, and SHS, are summarised in Table 1. All welds were prosecuted through the metal active gas welding process. As the component method can be used to design the bolted end plate connection, the main parameter investigated experimentally is the thickness of the end plate and the cover plate to verify the effectiveness of the component method. 'CCS' and 'WCS' denote the corner column splice and wall column splice, respectively. '6' and '8' represent the nominal thickness of the end plate and cover plate. 'A' and 'B' indicates repetitions of the same nominal specimens. For example, "WCS-6-A" is Wall column splice A with a nominal 6 mm end plate and cover plate.

M24 and M20 grade 10.9 hexagonal head bolts were used for the end plate and the cover plate, respectively. 200 Nm and 30 Nm torques were applied to the M24 bolt for specimens A and B, respectively, in order to evaluate the effect of the pretension load on the joint behaviour. The M20 bolts were tightened to 10 Nm. Note that a blind (or Hollo) bolt should be used to connect the cover plate and the lower hollow section (SHS2 in Fig. 4) in real construction. In the presented study, as blind bolts were not available at the time of experiments, the nuts of the M20 bolt were welded inside the hollow section before the end plate was welded. The cover plate was welded to the upper SHS in the factory and then connected to the lower SHS using M20 bolts. Since the bolt is used as a shear connector and the pretension load is very low, a neglectable difference is expected between the behaviour of the M20 bolt and the blind bolt.

Due to the asymmetric feature of the column splice, different elongations are expected on different sides of the column splice, resulting in a secondary bending of the specimen. A pin connection was used at the top and bottom of the specimen (see Fig. 4). The tail plate is welded along the axis of symmetry such that the specimen can be freely bent. The axis of symmetry is shown by the red dashed line in Appendix A.

2.2. Material mechanical properties

Three tensile coupon tests were conducted for each measured thickness following EN ISO 6892-1 [29]. The gauge length was 50 mm. The most representative engineering stress–strain curves for each thickness of the material are plotted in Fig. 5. The measured Young's modulus (E), yield strength (f_y), yield strain (ε_y), ultimate strength (f_u), ultimate strain (ε_u), strength ratio (f_u/f_y), and fracture at elongation (ε_f) are summarised in Table 2. Note that the stress–strain relationship of the 7.7 mm thick material does not have a yield plateau as the

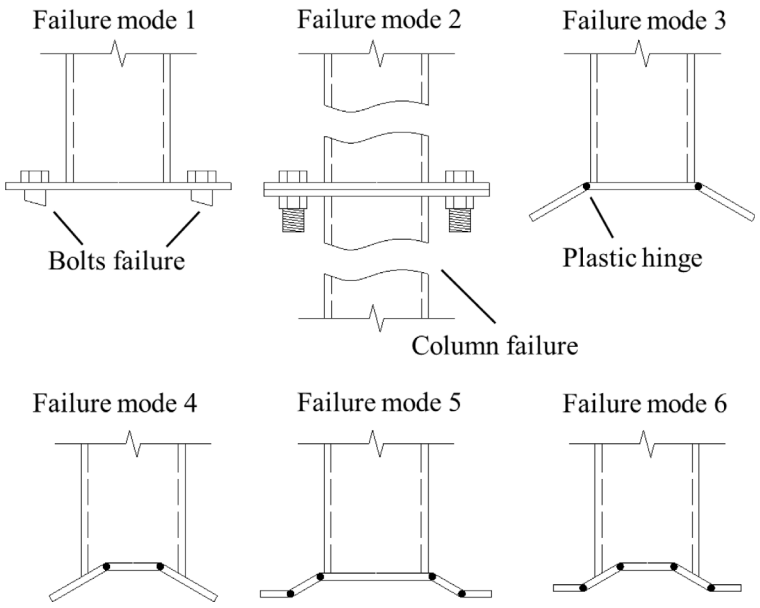

Fig. 2. Six failure modes of RHS two-side bolted column splices [13].

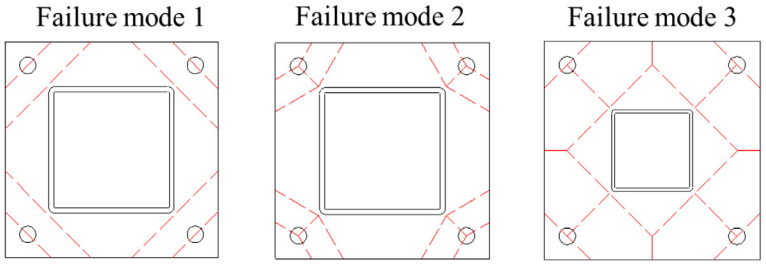

Fig. 3. Three failure modes with bolts positioned outside RHS dimension [21].

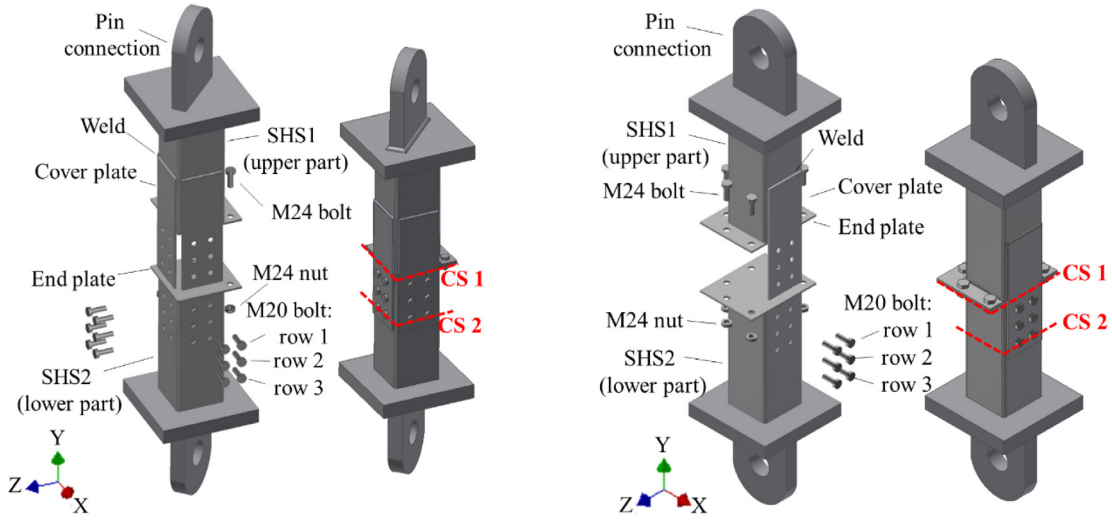

a) "Corner" column splice (CCS). b) "Wall" column splice (WCS).

Fig. 4. Column splices specimens.

Table 2
Mechanical properties.

Thickness [mm]	E [GPa]	f_y [MPa]	ε_y [%]	f_u [MPa]	ε_u [%]	f_u/f_y	ε_f [%]
6.0	193	404	0.209	574	14.07	1.42	28.9
7.7	194	479	0.447	583	8.56	1.28	23.7
7.9	197	361	0.183	551	16.11	1.53	27.1
8.5	200	391	0.196	562	14.08	1.44	30.8

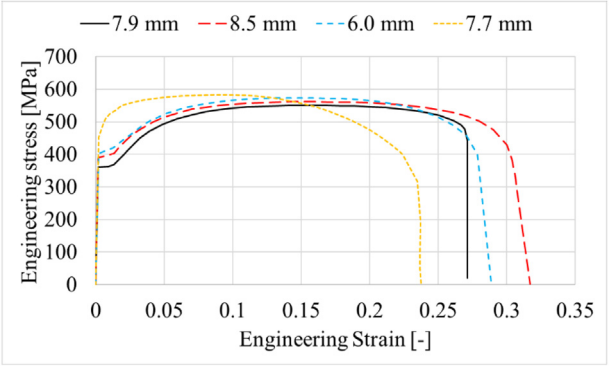

Fig. 5. Engineering stress–strain relationships.

coupon specimen was extracted from the cold-formed hollow section. The yield plateau is eliminated due to the cold-forming process. Hence, for 7.7 mm material, the yield stress is 0.2% proof stress, and the yield strain is $f_y/E+0.002$.

The true stress–strain relationship, including the descending part, derived from the engineering stress–strain relationship is used in the finite element (FE) analysis. It is worth mentioning that the true stress of the material should always increase with the increase of the true strain. However, since the material damage model is not included in this study, and the descending part of the stress–strain relationship would not influence the FE predicted ultimate resistance and deformation, the descending part of the true stress-true strain relationship is included in the FE analysis. The mechanical property of the weld is assumed to be identical to the tube property. Since negligible deformation was observed in the bolt, the nominal mechanical properties of the bolt (E = 200 GPa, f_y = 900 MPa, f_u = 1000 MPa) with an assumed 0.05 ultimate strain (ε_u) are used.

2.3. Test setup and program

Tensile tests were conducted in a setup with 2000 kN capacity at the Stevin lab II, TU Delft. The loading rates were 0.6 mm/min and 2 mm/min at the elastic and plastic stages. The plastic stage was identified when a significant deformation appeared in the measured load-deformation relationship during the test, e.g. around 1000 kN in Fig. 12(a), and the strain measured by the strain gauge was larger than 0.5%. Generally, the total time for testing a joint under static loading is around 1 h. The present study determined the loading rate based on the load-deformation relationship estimated by FEM before the test. As the cover plate was loaded in tension, it was more sensitive to the loading rate effect than the end plate connection. Hence, the strain measured from the strain gauge and the average deformation measured from LVDTs 3 and 4 were used to ensure the strain rate was lower than the up limit stipulated in ISO 6892-1 [29]. The test was terminated when the load decreased to 80% of the ultimate load.

The deformation of the specimen was measured by eight linear variable differential transformers (LVDTs) from Gefran during the experiment. Four LVDTs, namely L1–L4 shown in blue in Appendix B, were fixed on a bracket to measure the relative displacement between cross-sections A and B, which were 45 mm above and 90 mm below the contact surface of two end plates. The LVDTs were 185 mm away from the centre line of the tube. In order to evaluate the secondary bending effect during the tensile test, two horizontal LVDTs (H1 and H2 in red in Appendix B) were positioned against the cover plate at the mid-height of the specimen. The horizontal LVDT was held by a frame attached to a column which was connected to the ground, as shown in Fig. 6(a). A standard clearance bolt hole was used for M20 and M24. Hence, two LVDTs (S1 and S2 in green in Appendix B), glued to the surface of the lower hollow section, were used to measure the slip between the cover plate and the hollow section, which is the slip of the cover plate. Strain gauges from Tokyo Measuring Instrument Lab (FLAB-6-11) with a gauge length of 6 mm, namely SG1, SG2, and SG3 shown in Appendix B, were attached to the cover plate to evaluate the strain level. In addition, the deformation of the cover plate and the end plate were measured by 3D Digital Image Correlation (3D DIC). An example of testing CCS is shown in Fig. 6(a).

2.4. Finite element model

The commercial software ABAQUS 6.14 [30] is used to simulate the tensile behaviour of the column splice. The measured thickness in Table 1 and the nominal dimension in Appendix A are employed in the FE model. The fillet weld is generated by extruding an isosceles right triangular cross-section along the connected parts. A FE model of CCS is presented in Fig. 6(b) as an example.

Five pairs of surface-to-surface contact are involved in the model, as follows: the plate to the bolt head and nut contact, the end plate to the end plate contact, the cover plate to the tube contact, the bolt shank to the bolt hole contact and the tube to the end plate contact. The property of the contact pair contains a hard contact in the normal direction and a tangential contact with a 0.2 friction coefficient. The friction coefficient is determined according to the slip factor recommendation in EN 1090-2 [31]. The bolt consists of two parts which are a shank with a round head and a round nut. The washer is not created to simplify the model. A tie constraint is employed to fix the nut to the bolt shank. The two right-angle sides of the fillet weld are connected to the plate and SHS using the tie constraint.

The specimen is pin connected to the setup via two tail plates in the experiment, as shown in Fig. 6(a). For simplicity, the tail plate and the thick end plate (40 mm) are not included in the FE model. Two reference points (RP1 and RP2) are created at the centre of the top and bottom surfaces (Surface 1 and Surface 2), respectively. A rigid body constraint ties the reference point to the corresponding top or bottom surface. The displacement of RP1 in all three directions and RP2 in the X and Z directions are fixed. The load is applied by a displacement at RP2 in the Y direction.

A fine mesh (3 mm) is used for the critical part where the large deformation might occur, such as the end plate, the net cross-section of the top bolt row in the cover plate and the bottom bolt row in the column, as shown in Fig. 7. For the less important part in the cover plate and the column, a coarse mesh (9 mm) is adopted to improve the calculating efficiency. The tetrahedral C3D10M element is used for the transition part in the cover plate, which connects the fine and coarse mesh parts, see Fig. 7(a). The C3D8R element is used for the rest of the part (including the bolt and the weld) according to the recommendation from Bursi and Jaspart [32,33]. For all the mesh over the thickness, at least four elements are employed. The quasi-static analysis uses an explicit solver with a 100 s period and a 0.0001 s target time increment.

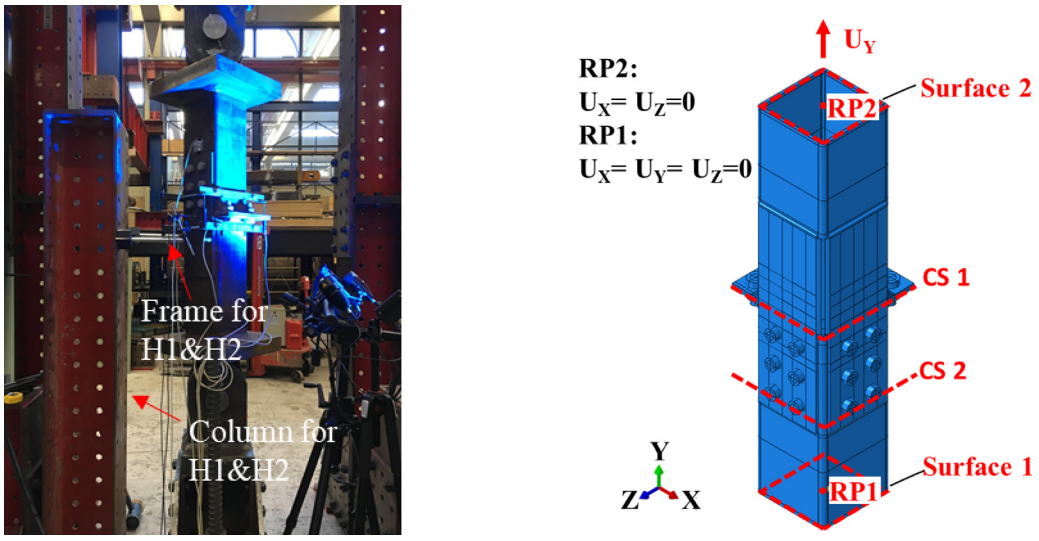

Fig. 6. An example of the corner column splice (CCS).

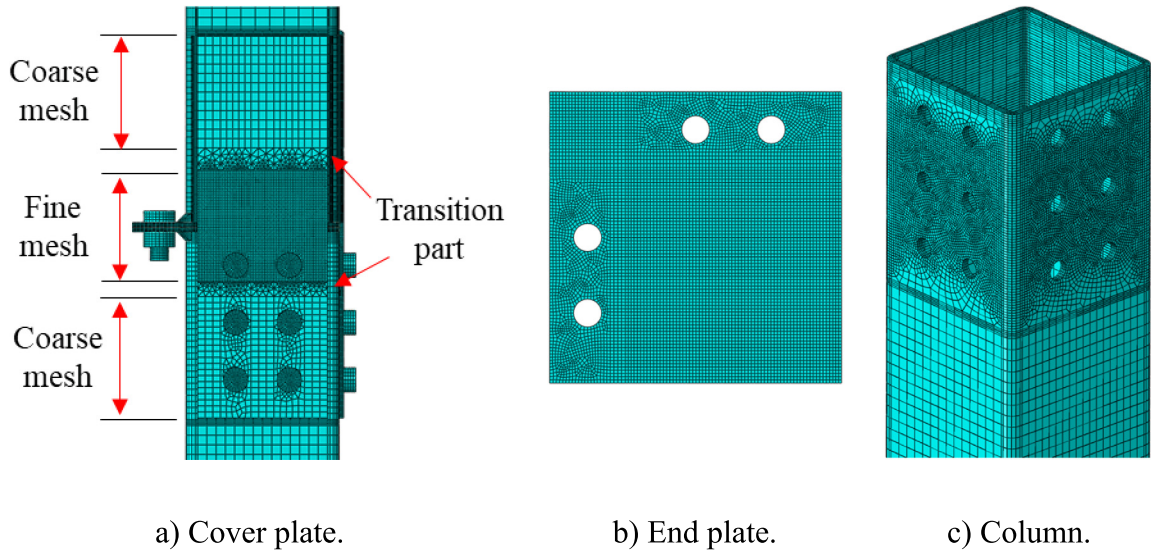

Fig. 7. Mesh details.

2.5. Mesh sensitivity verification

A mesh sensitivity investigation is carried out to verify whether the fine mesh size (3 mm) for the critical region is sufficient. Four mesh sizes (7 mm, 5 mm, 3 mm, and 2 mm) are investigated on the coupon specimen and joint levels. Fig. 8(a) compares the FE results to the experimental engineering stress–strain relationship (EXP). The FE prediction is independent of the mesh size at the elastoplastic stage. Since the material damage model is not included in the FE analysis, the mesh size influences the FE prediction after the ultimate point (with maximum strength). The model "fail" earlier with a finer mesh, indicating that the finer element is less "ductile". Fig. 8(b) presents the load-deformation relationship of the whole joint. With a coarser mesh, the FE model has a higher deformation capacity. The FE results show convergency when the mesh size is not greater than 3 mm at both coupon and joint levels. Therefore, a 3 mm mesh size is sufficient to predict the mechanical behaviour of the critical region.

3. Experimental and FE results

3.1. Failure modes

Two typical failure modes, which were the through-thickness fracture at the bolt row 1 net cross-section of the cover plate and fractures around washers at the end plate, were observed, as shown in Figs. 9 and 10. In the cover plate, as the net cross-section of bolt row 1 transfers the entire tensile force of the cover plate, resulting in the highest stress, the fracture is expected at this critical cross-section. However, the through-thickness fracture did not occur in the cover plate for the joint with two cover plates and 8 mm thick plates (CCS-8-B). A very clear necking appeared, and small cracks at the net cross-section were observed, as shown in Fig. 11. This was due to the less deformation capacity of the thick end plate (8 mm) than the thin end plate (6 mm), as the ultimate resistance of the end plate was reached at a deformation level lower than that of the cover plate. A detailed illustration of the failure mode is presented in Section 3.5. Negligible deformation was observed in the M24 and M20 bolts. The contour plot of equivalent plastic

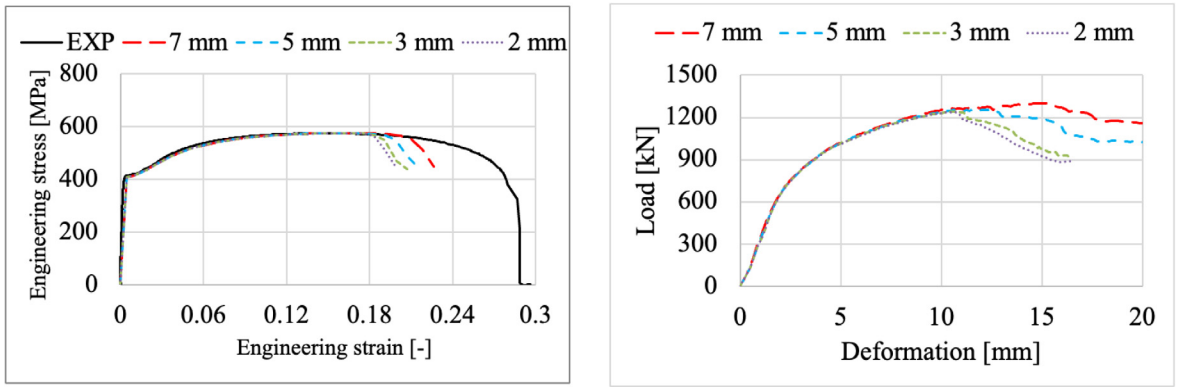

a) 6 mm thick coupon specimen. b) WCS-6 specimen.

Fig. 8. Mesh sensitivity investigation.

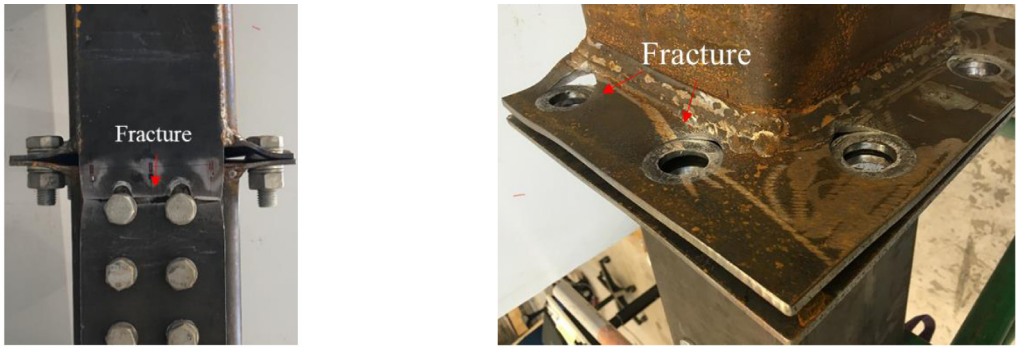

a) Fracture at the cover plate (EXP). b) Fracture at the end plate (EXP).

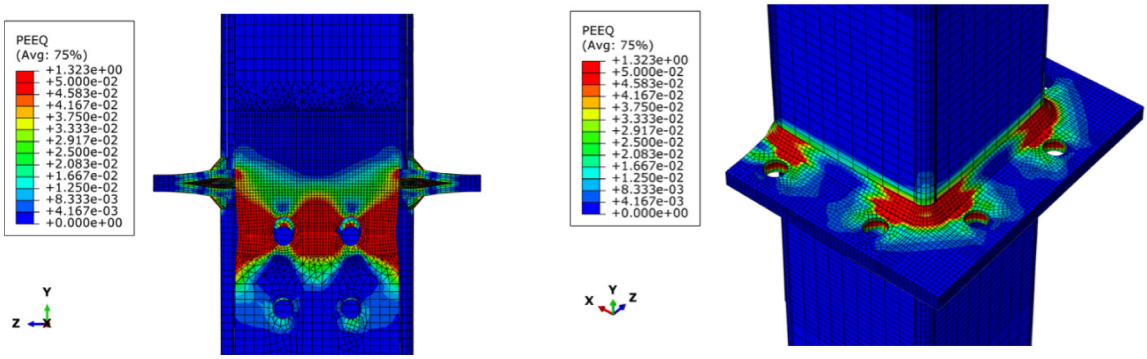

c) Fracture at the cover plate (FEM). d) Fracture at the end plate (FEM).

Fig. 9. Failure of Wall column splice (WCS-6-B).

strain (PEEQ) reveals the location of the fracture. The experimental and FE failure modes are compared in Figs. 9 and 10. The elements with high strain match well with the experimental fracture locations. It can be concluded that the failure mode of the specimen could be well predicted by FEM.

3.2. Load-deformation relationships

The load-deformation relationships obtained from FEM are compared to the experimental results in Fig. 12. The average deformation of LVDTs 1 and 2 describes the deformation on the end plate side, and the average deformation of LVDTs 3 and 4 represents the elongation of the cover plate. Very good agreements could be observed between the FE and the experimental results. The ultimate resistances obtained from FE models are averagely 2% higher than the experimental results, as shown in Table 3. Hence, it can be concluded that the FEM could reproduce the tensile behaviour of the column splice. Note that the specimen CCS-8-A is not considered due to premature failure in the heat-affected zone (HAZ), see Fig. 13. The fracture propagated along the toe of the weld. This failure mode might be due to the high heat

a) Fracture at the cover plate (EXP).

b) Fracture at the end plate (EXP).

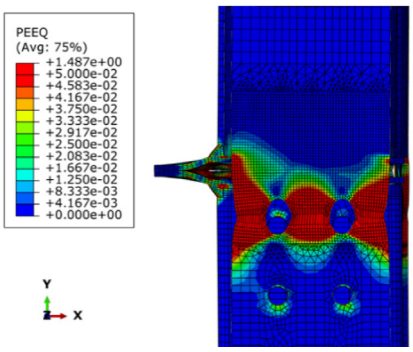

c) Fracture at the cover plate (FEM).

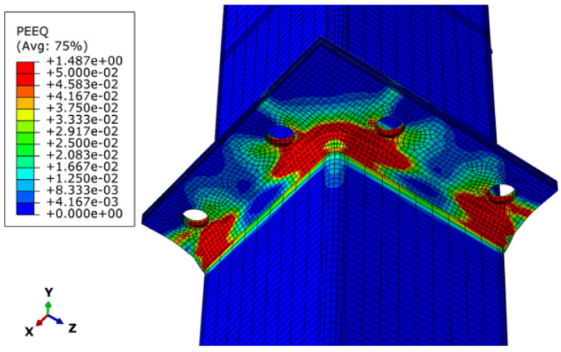

d) Fracture at the end plate (FEM).

Fig. 10. Failure of Corner column splice (CCS-6-B).

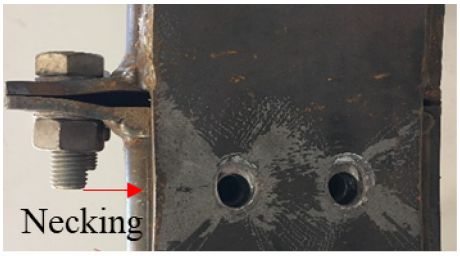

a) Necking of the cover plate.

b) Fracture inside the bolt hole.

Fig. 11. Failure of Corner column splice (CCS-8-B).

Table 3
Comparison of the ultimate resistance.

Specimens	WCS-6		WCS-8		CCS-6		CCS-8	
	A	B	A	B	A	B	A	B
$R_{u,EXP}$ [kN]	1200	1177	1543	1596	1403	1314	1345	1635
$R_{u,FEM}$ [kN]	1224		1559		1387		1746	
$R_{u,FEM}/R_{u,EXP}$	1.02	1.04	1.03	0.99	0.99	1.06	1.30	1.07

input during welding, as the mechanical properties of HAZ are sensitive to the maximum experienced temperature and the cooling time from 800 °C to 500 °C during welding [34], especially for high-strength steels [35]. However, the current design rule for the weld does not explicitly consider the material softening in HAZ, which might result in an unsafe prediction of the weld resistance.

In general, CCS and WCS show the same deformation trends in the slip (measured by S1 and S2) and horizontal displacement (measured by H1 and H2). Hence, the results of specimens WCS-6 are presented in Fig. 14 as examples. Fig. 14(a) depicts the relationship of the cover plate slip versus the load. Note that the data after the peak load is removed, as a significantly large value appeared at failure. The data point at failure would result in vague deformation details at the elastoplastic stage in the diagram. A limited slip was observed at the beginning of the test, indicating that the bolted end plate connection mainly carried the load due to the pretension load. Afterwards, the slip started to increase significantly. It can be seen that specimen A has a higher load at the slip initiation than specimen B (at a load of 150 kN

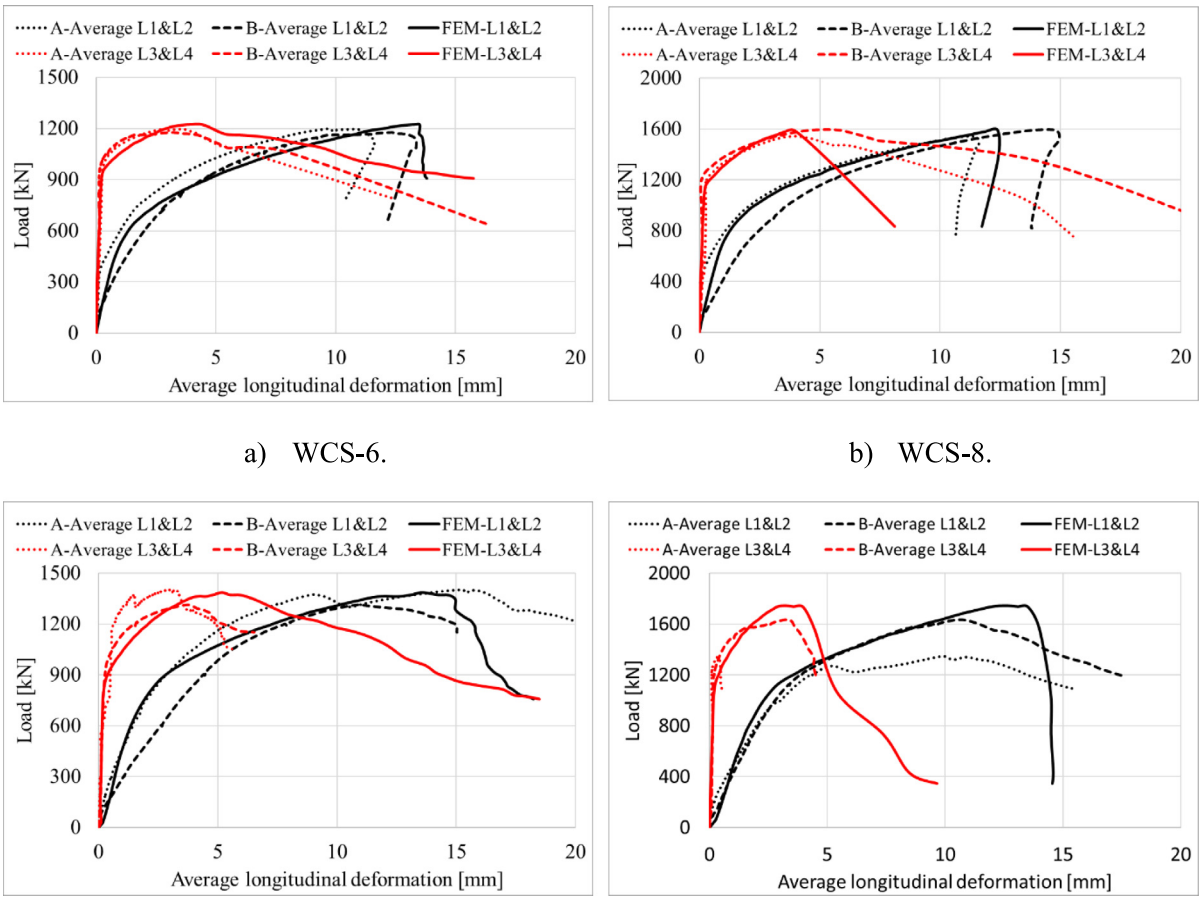

Fig. 12. Comparison of load-deformation relationships.

for specimen A and 40 kN for specimen B). The reason is that a higher pretension load was applied on the M24 bolt in specimen A than in specimen B. The slope of the load-slip relationship increases around 1 to 2 mm due to the ordinary 2 mm bolt-hole clearance.

The load-horizontal displacement relationships are plotted up until the peak load in Fig. 14(b). A limited horizontal displacement, less than 0.4 mm, was observed when the load increased to approximately 150 kN and 40 kN for specimens A and B, respectively. The difference is caused by the different levels of pretension. Firstly, the specimen bent towards the side with the cover plate due to the clearance in the cover plate bolt hole. After a 1–2 mm slip referring to Fig. 14(a), the specimen gradually stopped bending to the cover plate side. When the load is higher than 800 kN, the specimen deformed away from the cover plate side due to the yielding of the cover plate.

The load against the longitudinal strain ε_{yy} in the cover plate of specimen WCS-6-B are plotted in Fig. 15. Theoretically, a larger strain is expected at SG1 and SG3 than SG2, as SG1 and SG3 are closer to the weld. However, the strain measured at SG1 and SG2 were larger than SG3 at the elastic stage. The slip at WCS-6-B-S2 was larger than WCS-6-B-S1, see Fig. 14(a), indicating that the SG1 side was activated earlier than the SG3 side. It is, therefore, reasonable to have a smaller strain at SG3 at the elastic stage. After the cover plate yields, the strain at SG1 and SG3 increased much faster than at SG2. The diagrams indicate that the cover plate yields around 800 kN, which explains the reversed horizontal deformation mentioned above.

3.3. Equivalent deformation of the whole column splice

The equivalent deformation of the whole column splice is evaluated by the deformation between cross-sections A and C shown in Appendix B. The total deformation on the cover plate side consists of the elongation of the cover plate and the slip between the cover plate and the SHS. The total slip and the elongation of the cover plate between cross-sections A and B were measured, while the elongation between cross-sections B and C is unknown. However, the slip and the localised plastic deformation at bolt row 1 govern the total deformation of the cover plate side at the elastic and the plastic stage, respectively. It can be proved by the FE result, where the deformation between cross-sections B and C is always less than 0.2 mm. Hence, the elongation between cross-sections B and C is excluded from the equivalent deformation.

The deformation was measured between cross-sections A and B on the end plate side. The elongation of the tube between cross-sections B and C is unknown. As the yield resistance of the SHS is much higher than the peak load of the test, a negligible elastic deformation is expected in the SHS between cross-sections B and C. Hence, the deformation between cross-sections B and C is excluded from the total deformation on the end plate side. The equivalent deformation of the column splice can be calculated by the following expression:

$$\Delta_j = \frac{\frac{\Delta_{L1}+\Delta_{L2}}{2} + \left(\frac{\Delta_{L3}+\Delta_{L4}}{2} + \frac{\Delta_{S1}+\Delta_{S2}}{2}\right)}{2} \quad (1)$$

where Δ_{Li} and Δ_{Si} are the deformations measured by LVDTs L_i and S_i, respectively.

3.4. Effect of different parameters

Fig. 16 presents the load-equivalent deformation curves of WCS and CCS. The ultimate resistance and stiffness of each test are summarised

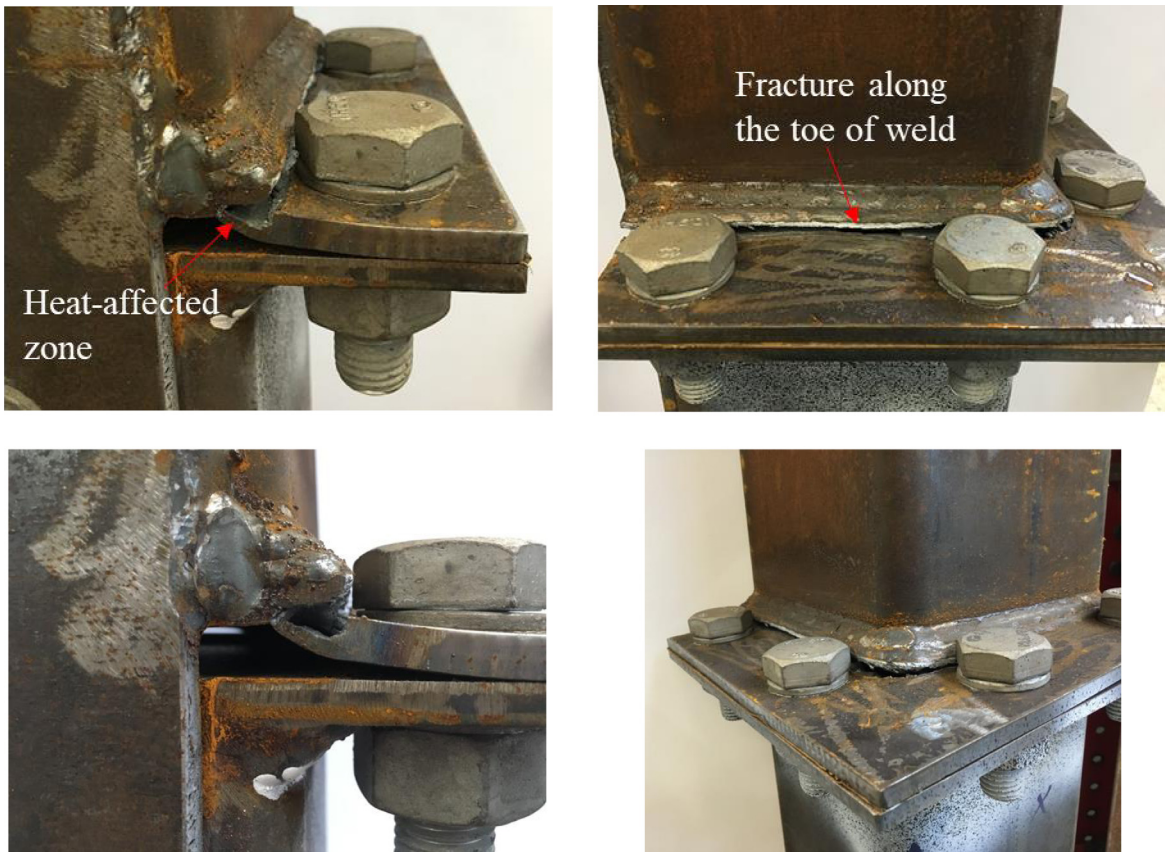

Fig. 13. Premature failure in the heat-affected zone of CCS-8-A.

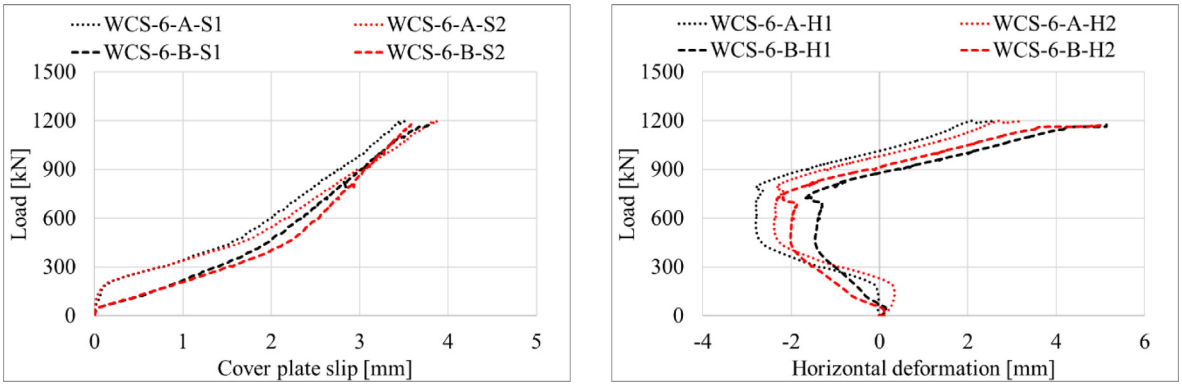

a) Slip displacement (S1, S2). b) Horizontal displacement (H1, H2).

Fig. 14. Load–displacement relationships of WCS-6 specimens.

in Table 4. Note that the data of specimen CCS-6-A is not available due to the missing slip data. The ultimate resistance of the specimen CCS-8-A is excluded from the discussion because of the premature failure in HAZ. With a 2 mm increment of the plate thickness, the ultimate resistance of WCS and CCS increases by 32% and 20%, respectively; the stiffness increases by 38% and 57% for WCS and CCS, respectively. A relatively small difference could be obtained between WCS and CCS with the same plate thickness. CCS has a 9% and 13% higher ultimate resistance and stiffness compared to WCS, respectively, as the cover plate in tension has a higher resistance and stiffness compared to the end plate in bending. A considerable deformation occurred when the load was around 150 kN for specimens A and 40 kN for specimens B.

Comparing the ultimate resistance of specimen B to Specimen A, the maximum difference is less than 6% (excluding specimen CCS-8-A), indicating that the pretension load does not influence the ultimate resistance. The reason is that the end plate and the cover plate govern the failure, which is independent of the pretension load. In the case of the end plate equivalent T-stub, the bolt did not show any plastic deformation, indicating that failure mode 1 (complete yielding of the end plate) occurred. The resistance of failure mode 1 is not dependent on the pretension load. The pretension load in the T-stub does not affect the resistance of the cover plate.

As the stiffness of CCS-6-A is not available and CCS-8-A has a premature failure, WCS specimens are used to evaluate the effect of pretension load on joint stiffness. Table 4 shows that the stiffness

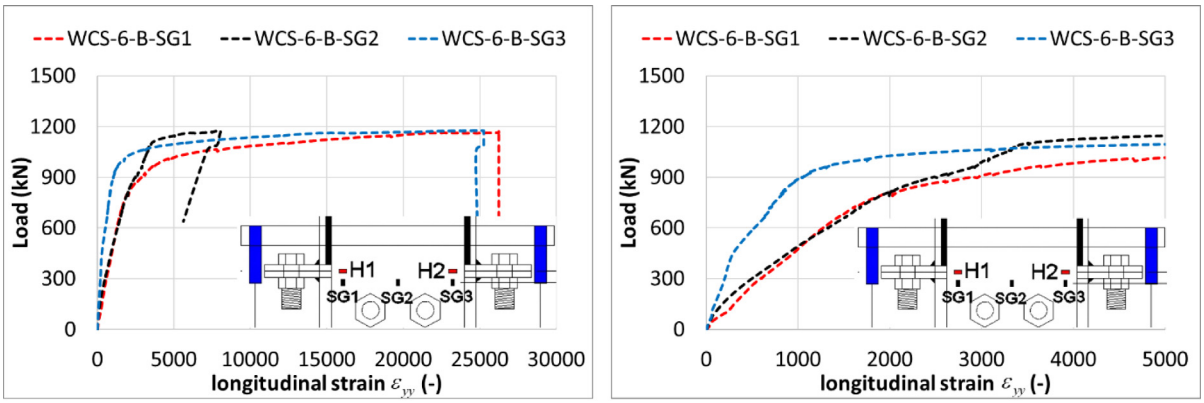

a) Overview of strain development. b) Detail of strain development.

Fig. 15. Load–strain relationships of WCS-6-B (SG1, SG2, SG3).

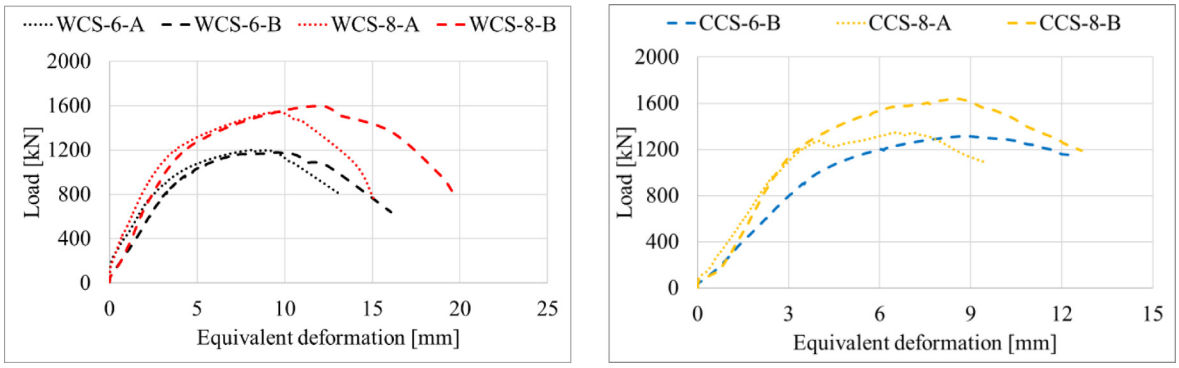

a) Wall column splice. b) Corner column splice.

Fig. 16. Load-equivalent deformation relationships.

Table 4
The ultimate resistance and stiffness for tested specimens.

Specimens	WCS-6		WCS-8		CCS-6		CCS-8	
	A	B	A	B	A	B	A	B
Ultimate resistance $R_{u,EXP}$ (kN)	1200	1177	1543	1596	1403	1314	1345	1635
Stiffness $S_{j,ini,EXP}$ (kN/mm)	256	252	348	354	–	269	379	463

difference between Specimen A and B is less than 3%. However, it is worth mentioning that the pretension load level is relatively low. The pretension load might be influential if the load level is higher.

3.5. Different deforming stages of the column splice (3D DIC results)

The equivalent strain contour plot of CCS-6-A at the peak load is shown in Fig. 17(a). The strain exceeding 5% mainly appears at the net cross-section of bolt row 1. Hence, the strain ε_{yy} is extracted from nine data points uniformly distributed at the net cross-section. The average strain $\bar{\varepsilon}_{yy}$ of nine data points is employed to estimate the force in the cover plate, referring to the material stress–strain relationship. Assuming that two cover plates in specimen CCS-6-A carried the same load, the load distributed in the cover plate and in the bolted end plate connection is calculated.

As the equivalent deformation of the specimen CCS-6-A is unavailable, the total displacement from the jack is used in Fig. 17(b). The DIC data is available when the load is beyond 145 kN. Six red points, representing six deforming moments, are characterised as follows: the initiation of the cover plate slip, the end of the major cover plate slip, the full activation of the cover plate, the yielding of the cover plate, the failure of the end plate, and the failure of the cover plate. Details of each deforming stage are explained below.

(1) Stage 1 (up to Point 1): The load was carried by the bolted end plate connection. The horizontal displacement and the cover plate slip were minor. The pretension load caused a delay in the deformation initiation.

(2) Stage 2 (Point 1–Point 2): The cover plate slip occurred at this stage. The slip and the horizontal displacement increased with the ascending load. Note that a small gap might still exist for a few bolt holes at the end of this stage, indicating that the cover plate was not completely activated.

(3) Stage 3 (Point 2–Point 3): The load in the cover plate and end plate increased at approximately the same rate. It indicates that the stiffness of the cover plate side and the end plate side are very close, which also explains the constant horizontal deformation between 400 kN–700 kN, shown in Fig. 14(b). All bolts touched the bolt hole, and the cover plate was fully activated at the end of this stage.

(4) Stage 4 (Point 3–Point 4): The cover plate carried most of the increasing load, while the end plate kept deforming without increasing

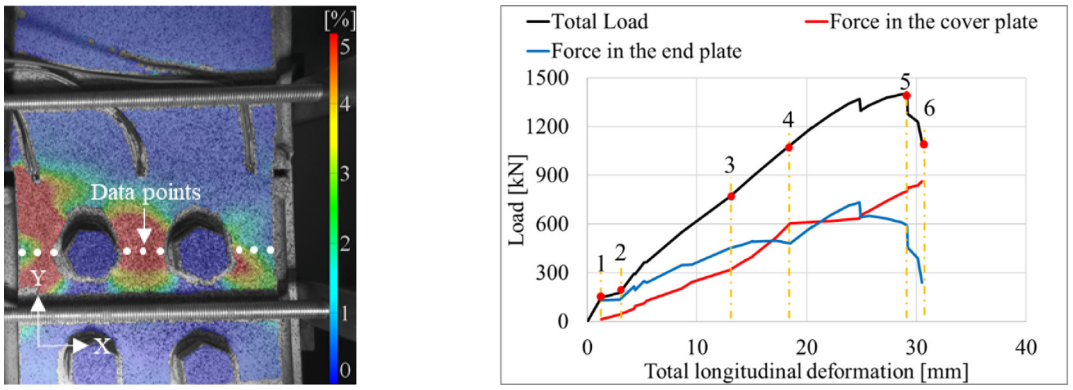

a) Strain contour plot. b) Load-deformation curves.

Fig. 17. Internal force distribution of specimen CCS-6-A. (For interpretation of the references to colour in this figure legend, the reader is referred to the web version of this article.)

force. Due to the stiffness difference, the specimen deformed away from the cover plate side, see Fig. 14(b).

(5) Stage 5 (Point 4–Point 5): At Point 4, the cover plate yielded at the net cross-section of bolt row 1. The increasing load was mainly carried by the end plate. When the ultimate resistance of the end plate was reached, corresponding to the first load drop at 1375 kN, the internal force redistribution started. The force carried by the end plate decreased with the fracture propagation in the end plate, while the force in the cover plate increased significantly. When the increasing load rate in the cover plate was less than the decreasing load rate in the end plate, the ultimate resistance of the column splice was reached.

(6) Stage 6 (Point 5–Point 6): After the ultimate resistance, most of the load is gradually redistributed to the cover plate. As the ultimate resistance of the cover plate was reached, the final failure of the column splice occurred, accompanied by a substantial horizontal movement towards the cover plate side. However, the through-thickness fracture in the cover plate might not appear if the fracture propagates quickly in the end plate, which is the case for CCS-8.

4. Discussions

4.1. Characterisation of the yield resistance

Yan et al. [36] proposed a bi-linear model to characterise the joint yield resistance, as shown in Fig. 18. The bi-linear model could describe the full-range behaviour, which is suitable for an elasto-plastic global analysis [4]. The initial stiffness ($S_{initial}$) line is used as a reference. The plastic behaviour is represented by an inclined line ending at the ultimate resistance (R_u) point. The yield resistance (R_y) is determined by moving the intersection point of elastic and plastic lines until two hatched blue areas are equal. The bi-linear model is adopted in this paper. The characterised yield resistance for each specimen is shown in Fig. 21 and Table 7.

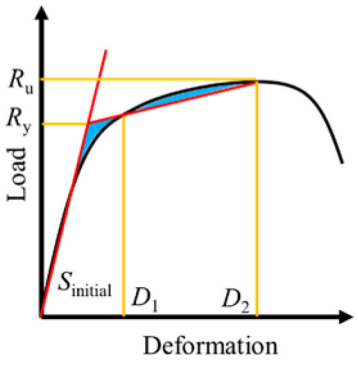

Fig. 18. Bi-linear model. [36].

4.2. Prediction of the component method

The component method (CM) [9] is employed to predict the column splice resistance. The resistance is determined by the lower resistance at two critical Cross-Sections (CS1 and CS2), as shown in Fig. 6(b). A schematic drawing for each employed component is presented in Appendix C. The red dash line represents the critical cross-section. The resistance of the end plate side and the cover plate side should be checked at CS1. Seven components are involved on the cover plate side, as follows:

- Component 9 — Plate in tension (cover plate)
- Component 12 — Bolts in bearing (cover plate)
- Block tearing failure of the cover plate
- Component 11 — Bolts in shear
- Component 12 — Bolts in bearing (column)
- Block tearing failure of the column
- Component 19 — Welds (cover plate)

The component plate in tension (cover plate) is used to check the resistance of the net and gross cross-section of the cover plate. The bearing resistance of the bolt hole in the cover plate and the column is considered by Component 12. The block tearing failure of the cover plate and the column is also considered in the resistance prediction.

Three components are involved on the end plate side:

- Component 5 — End plate in bending
- Component 10 — Bolts in tension
- Component 19 — Welds (end plate)

At CCS2, the tensile resistance is governed by the column, which could be designed by the component plate in tension for the whole column cross-section.

- Component 9 — Plate in tension (column)

The design equations in prEN1993-1-8 [9] are used to calculate the resistance of all involved components, except for the effective yield line length of the component end plate in bending. Steige and Weynand [16] proposed equations for the effective length at the corner of the end plate. The yield line pattern and the design equations are shown in Fig. 19 (red lines) and Table 5, respectively. The edge bolt is the bolt close to the flushed edge of the end plate. The rest of the bolts are called the corner bolt. The original equations in [16] allow

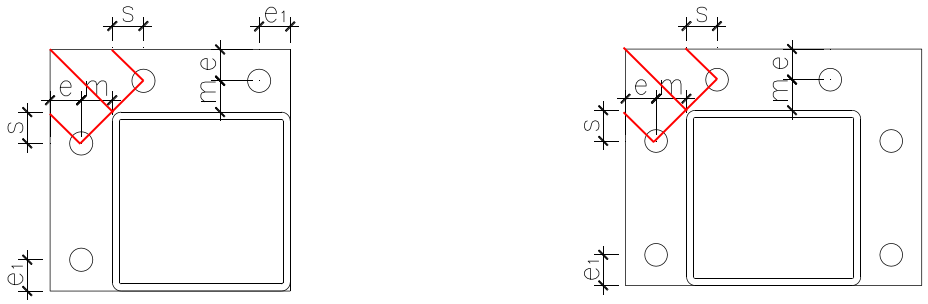

a) Dimensions of the corner column splice. b) Dimensions of the wall column splice.

Fig. 19. Yield line model with dimensions of Eqs. Eq. (2) and (3). (For interpretation of the references to colour in this figure legend, the reader is referred to the web version of this article.)

Table 5
Effective length of the yield line [9,16].

Failure type	Bolt location	$l_{\mathrm{eff,cp}}$(Circular patterns)	$l_{\mathrm{eff,nc}}$(non-Circular patterns)
Bolt considered individually	Edge bolt	The smaller of: $2\pi m; \pi m + e_1$	The smaller of: $4m + 1.25e; 2m + 0.625e + e_1$
	Corner bolt	The smaller of: $2\pi m; \pi m + e_1$	The smaller of: $4m + 1.25e; 2m + 0.625e + l_{\mathrm{eff,i}}$
Bolt considered as part of group bolts	Edge bolt	The smaller of: $\pi m + p; p + 2e_1$	The smaller of: $2m + 0.625e + 0.5p; e_1 + 0.5p$
	Corner bolt	$\pi m + p$	The smaller of: $2m + 0.625e + 0.5p; 0.5p + l_{\mathrm{eff,i}}$

Table 6
Comparison of the effective yield line length.

Type	No.	Corner bolt			Edge bolt		
		$l_{\mathrm{eff,equ}}$ [mm]	$l_{\mathrm{eff,mea}}$ [mm]	$\frac{l_{\mathrm{eff,equ}}}{l_{\mathrm{eff,mea}}}$	$l_{\mathrm{eff,equ}}$ [mm]	$l_{\mathrm{eff,mea}}$ [mm]	$\frac{l_{\mathrm{eff,equ}}}{l_{\mathrm{eff,mea}}}$
WCS-6	A B	136	276	0.49	100	167	0.60
WCS-8	A B	137	255	0.54	100	174	0.58
CCS-6	A B	137	282	0.49	100	183	0.55
CCS-8	A B	136	287	0.47	100	210	0.48

for different m and e values on different RHS sides. Since m and e are constant on different SHS sides in this study, the original equations are simplified, as presented in Eqs. Eq. (2) and (3). The parameters m, e, s and e_1 denote the distance from the centre of the bolt hole to the yield line beneath the weld, to the edge of the end plate, to the edge of the tube (end plate side), and to the edge of the tube (cover plate side), respectively, as shown in Fig. 19.

$$x = \frac{1}{2m}\left[-2es + \left(4e^2s^2 + 4mes^2 + 4m^2e^2 + 4em^3 + 4me\,(-s+m)\,(m+e)\right)^{\frac{1}{2}}\right] \tag{2}$$

$$l_{\mathrm{eff,i}} = \frac{1}{4mx + 4es}\left[2me^2 + 2mx^2 2smx + 4es^2 + 2m\,(m+e)\,(x+e) + 2em^2\right] \tag{3}$$

In addition to the equations presented above, the effective yield line length is directly measured from the validated FE model. The yield line is the boundary of the yield region, indicating where the plastic hinge occurs. As the whole cross-section of the plastic hinge yields, the equivalent plastic strain (PEEQ) in the end plate central layer at the ultimate load is investigated, as presented in Fig. 20. 0.2% PEEQ is adopted as the critical yield strain. The yield region with PEEQ larger than 0.2% is in red. The boundary of the yield region is depicted by the black line (yield line). The effective yield line length is estimated by measuring the length of the black yield line.

Table 6 compares the effective lengths derived from the analytical equations ($l_{\mathrm{eff,equ}}$) and measured from the FE results ($l_{\mathrm{eff,mea}}$). It can be seen that the measured length is approximately two times the calculated length. Besides, a group non-circular yield pattern involving two bolts on the same SHS side is predicted following . However, the FE result shows two bolts close to the same corner fail as a group (within one yield region), while the bolts on the same SHS side yield separately. A circular yield pattern could be observed from all FE models. The calculated resistance for each specimen is shown in Fig. 21 and Table 7.

4.3. Comparison of column splice resistances

The column splice resistances determined by the bi-linear model (R_y), the component method using $l_{\mathrm{eff,equ}}$ ($R_{\mathrm{CM,equ}}$), and the component method using $l_{\mathrm{eff,mea}}$($R_{\mathrm{CM,mea}}$) are compared to the experimental results in Fig. 21 and Table 7. In addition, based on the validated FE models, the FE analysis using the perfect elasto-plastic constitutive model ($\mathrm{FE_{eltopl}}$) is conducted to provide a conservative estimation for each configuration. The perfect elasto-plastic constitutive model has the same yield strength as the test result but without the material hardening.

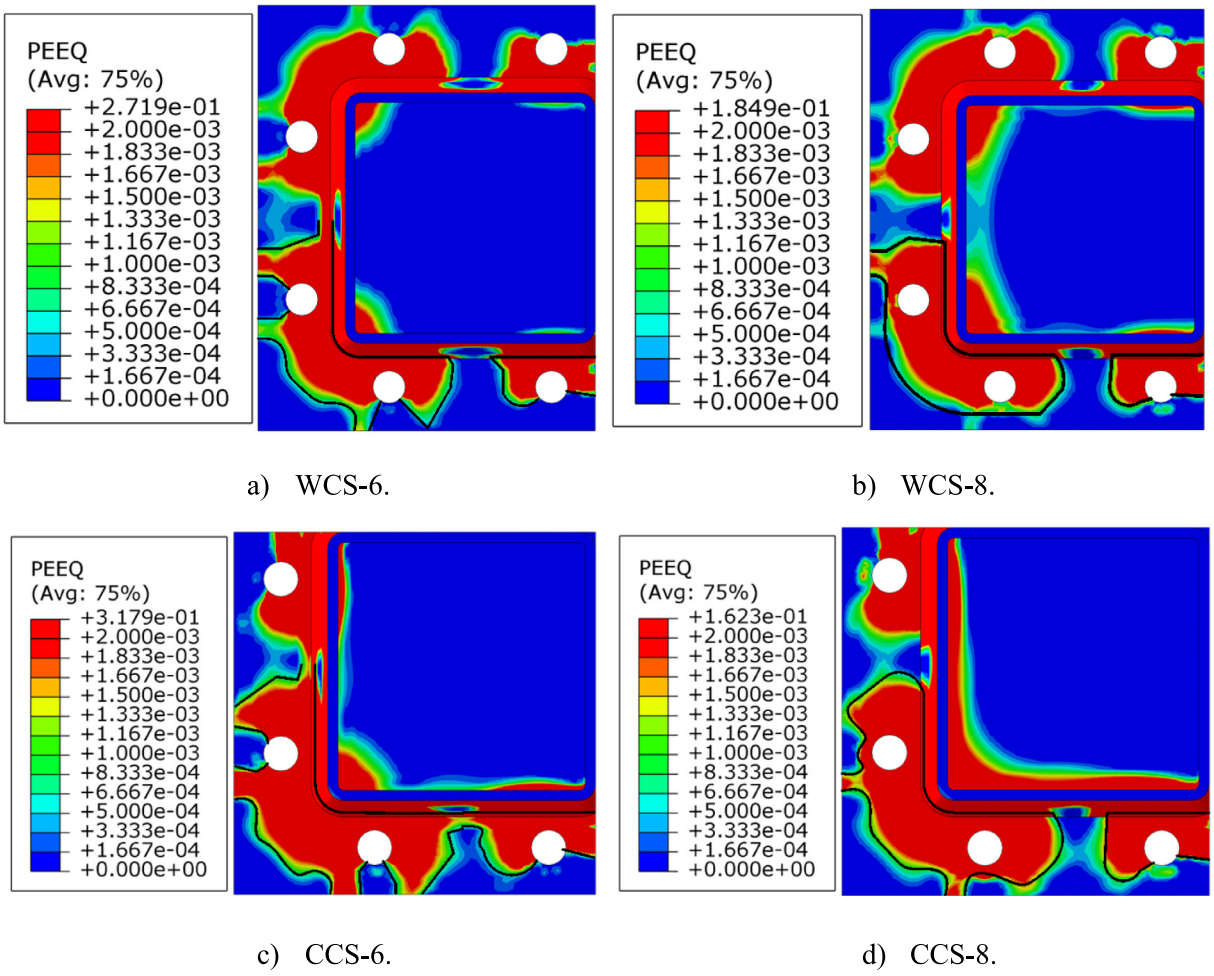

Fig. 20. Yield line at the middle-thickness cross-section. (For interpretation of the references to colour in this figure legend, the reader is referred to the web version of this article.)

Table 7
Comparison of the column splice resistance.

Type	No.	Experiment [kN]		Component method [kN]		Ratio			
		R_u	R_y	$R_{CM,equ}$	$R_{CM,mea}$	$\frac{R_{CM,equ}}{R_u}$	$\frac{R_{CM,mea}}{R_u}$	$\frac{R_{CM,equ}}{R_y}$	$\frac{R_{CM,mea}}{R_y}$
WCS-6	A	1200	965	531	738	0.44	0.62	0.55	0.76
	B	1177	1018			0.45	0.63	0.52	0.72
WCS-8	A	1543	1183	818	1162	0.53	0.75	0.69	0.98
	B	1596	1245			0.51	0.73	0.66	0.93
CCS-6	A	1403	–	760	908	0.54	0.65	–	–
	B	1314	1083			0.58	0.69	0.70	0.84
CCS-8	A	1345	–	1056	1313	0.79	0.98	–	–
	B	1635	1324			0.65	0.80	0.80	0.99

As CCS-8-A had a premature failure in HAZ, it is excluded from the following discussion, although the calculated resistances ($R_{CM,equ}$ and $R_{CM,mea}$) are still safe. Fig. 21 shows that the bi-linear model characterises a yield resistance R_y closing to the ultimate stage of FE_{eltopl}, indicating that the benefit of material strain hardening is excluded from R_y. The characterised yield resistance is well predicted using the measured effective length. $R_{CM,mea}$ is averagely 13% lower than R_y with a varying range of 1% to 28%. However, $R_{CM,equ}$ is significantly lower than R_y by 35% on average. Compared to the ultimate resistance (R_u) of the column splice, $R_{CM,equ}$ and $R_{CM,mea}$ are lower by 47% and 31% on average.

5. Conclusions

Two new asymmetric bolted column splices for square hollow sections (SHS) are proposed in this paper. The generic tensile behaviour of the column splices is studied through the experiments, the finite

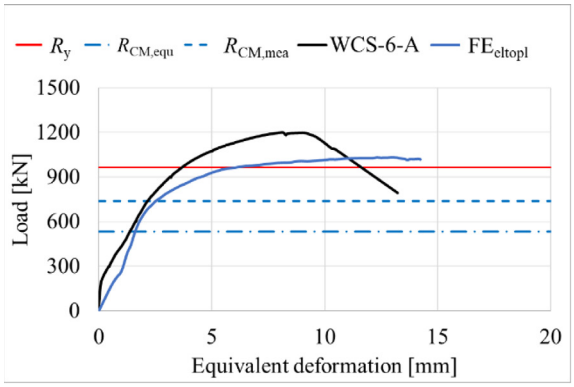

a) Specimen WCS-6-A.

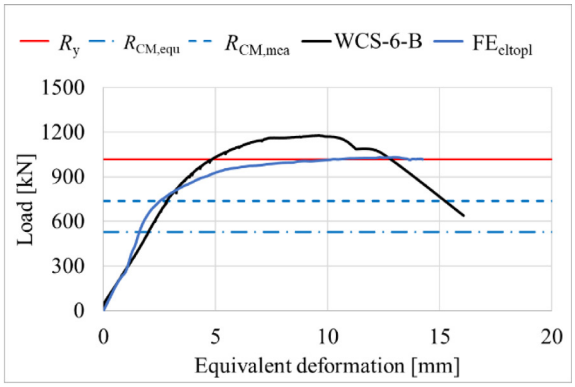

b) Specimen WCS-6-B.

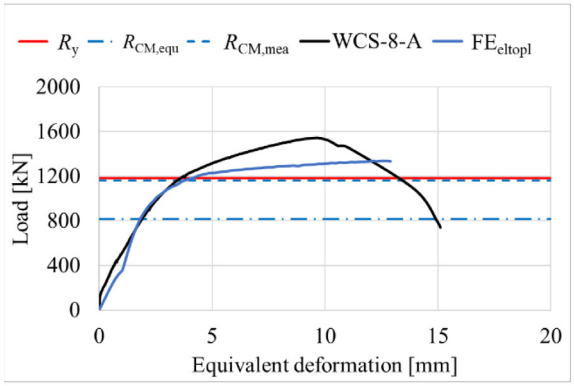

c) Specimen WCS-8-A.

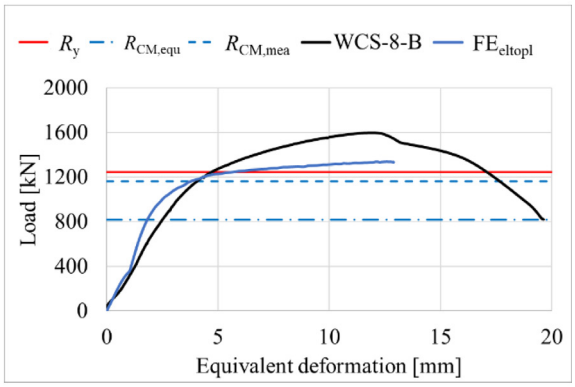

d) Specimen WCS-8-B.

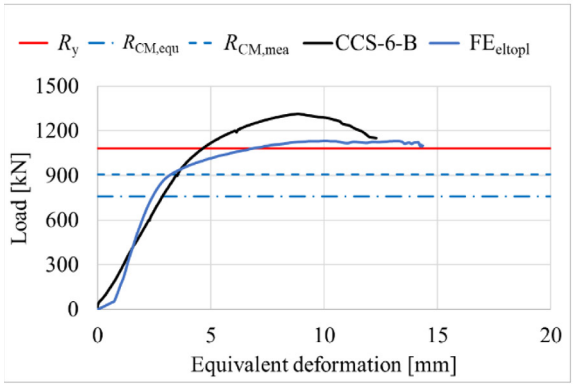

e) Specimen CCS-6-B.

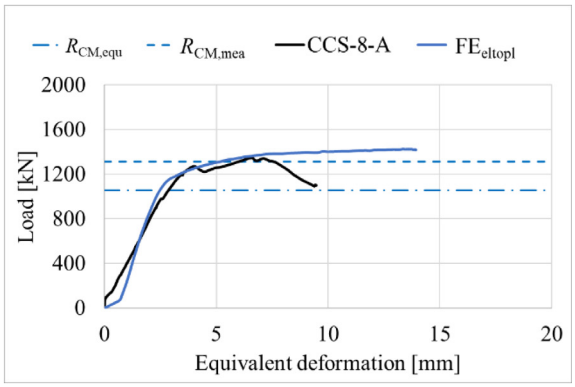

f) Specimen CCS-8-A.

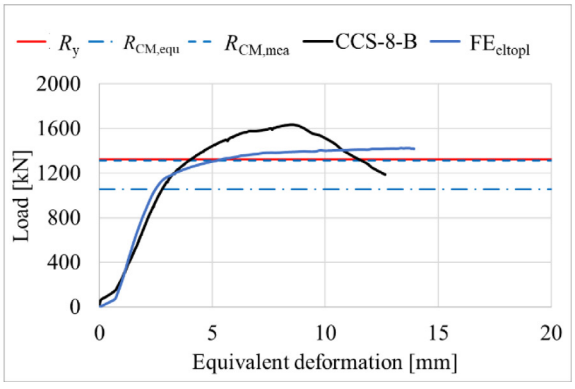

g) Specimen CCS-8-B.

Fig. 21. Comparison of the column splice resistance.

element (FE) analysis, and the analytical model (component method). Based on the presented results, the following conclusions are drawn:

1 With a 2 mm thicker end plate and cover plate (from 6 mm to 8 mm), the average ultimate resistances increase by 32% and 20% for the wall column splice (WCS) and the corner column splice (CCS), respectively.
2 The pretension load in the bolts on the end plate may delay the initiation of the column splice deformation. However, it does not influence the ultimate resistance.
3 A bi-linear model is used to characterise the yield resistance (R_y) of the column splice. R_y is very close to the ultimate resistance of the finite element model using the perfect elasto-plastic constitutive model, indicating that the benefit of material strain hardening is excluded from R_y.
4 The component method could be used to design the asymmetric column splices. The effective yield line length measured from the validated FE model is approximately two times the length calculated by the analytical equations. Using the measured effective length, the component method predicts an averagely 13% lower resistance than R_y, with a varying range of 1% to 28%. Using the calculated effective length, the joint resistance is significantly underestimated by 47% on average, compared to the joint ultimate resistance (R_u).
5 The analytical equations for effective length predict a non-circular group failure mode involving two bolts on the same SHS side, while a group circular failure mode at the corner of the end plate is observed in FE results.

The design rules for bolted end plate column splices with RHS and SHS are unavailable in the design code. The analytical model in the literature predicts a conservative effective length, resulting in a significantly lower resistance than the experiments. And the predicted yield pattern on the end plate differs from the validated FE results. For future work, the equations for calculating the effective length should be updated, and a realistic yield region of the end plate should be supplemented to the current specification. These should be accomplished by a comprehensive parametric study.

CRediT authorship contribution statement

Rui Yan: Writing – review & editing, Writing – original draft, Visualization, Validation, Methodology, Investigation, Formal analysis, Data curation, Conceptualization. **Haohui Xin:** Writing – review & editing, Writing – original draft, Supervision. **Milan Veljkovic:** Writing – review & editing, Supervision, Funding acquisition. **Luís Simões Da Silva:** Writing – review & editing, Supervision, Funding acquisition.

Declaration of competing interest

The authors declare that they have no known competing financial interests or personal relationships that could have appeared to influence the work reported in this paper.

Data availability

Data will be made available on request.

Acknowledgements

The research presented in this paper is based on the results of the INNO3DJOINTS project. The work was supported by the RFCS [grant numbers 749959]. The financial support is thereby gratefully acknowledged.

Appendix A. Nominal dimensions of each component [mm].

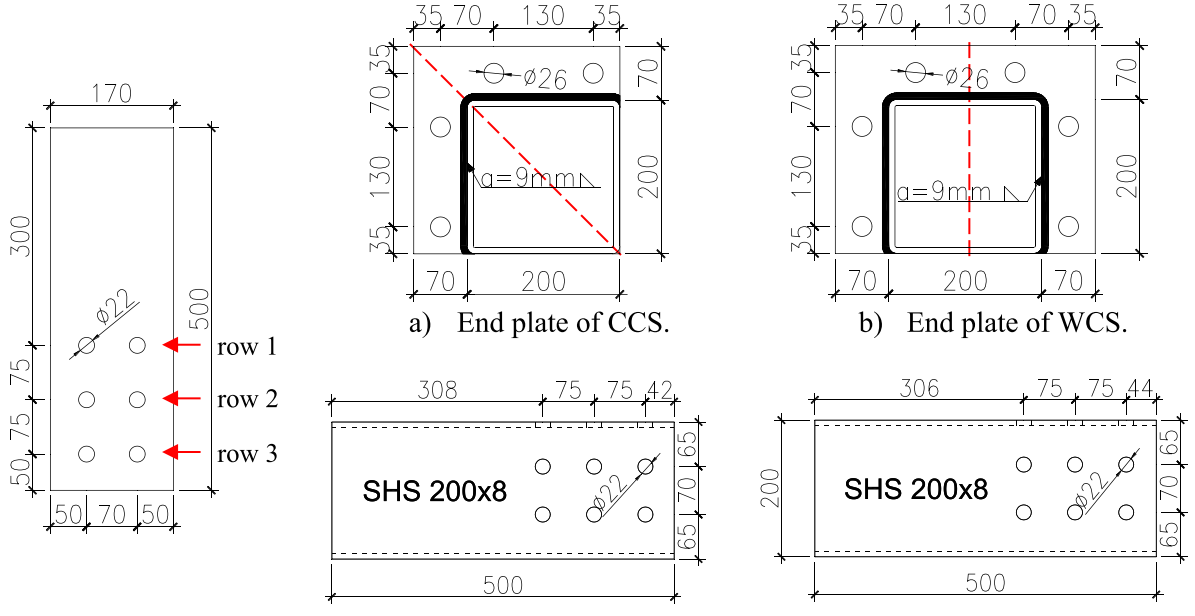

a) End plate of CCS.
b) End plate of WCS.
c) Cover plate.
d) Column for specimen with 8 mm end/cover plate.
e) Column for specimen with 6 mm end/cover plate.

Appendix B. Arrangement of LVDTs [mm].

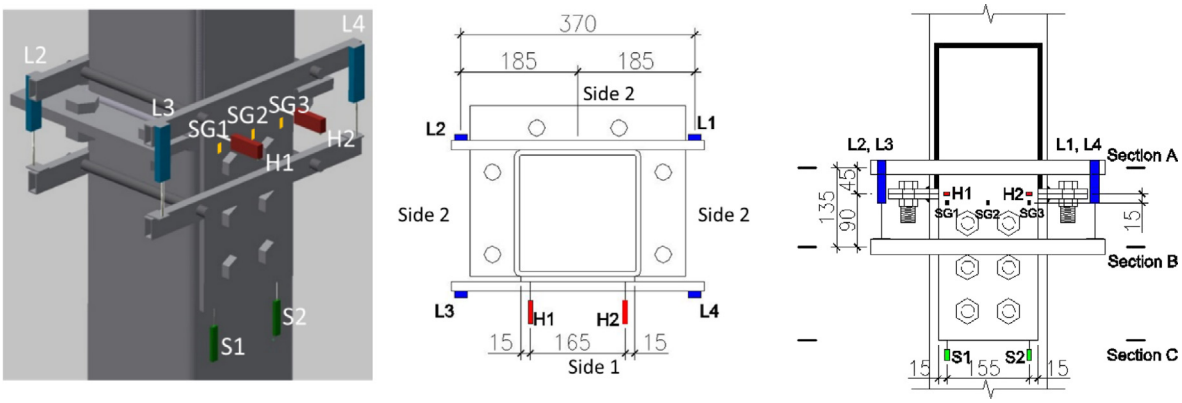

a) Wall column splice.

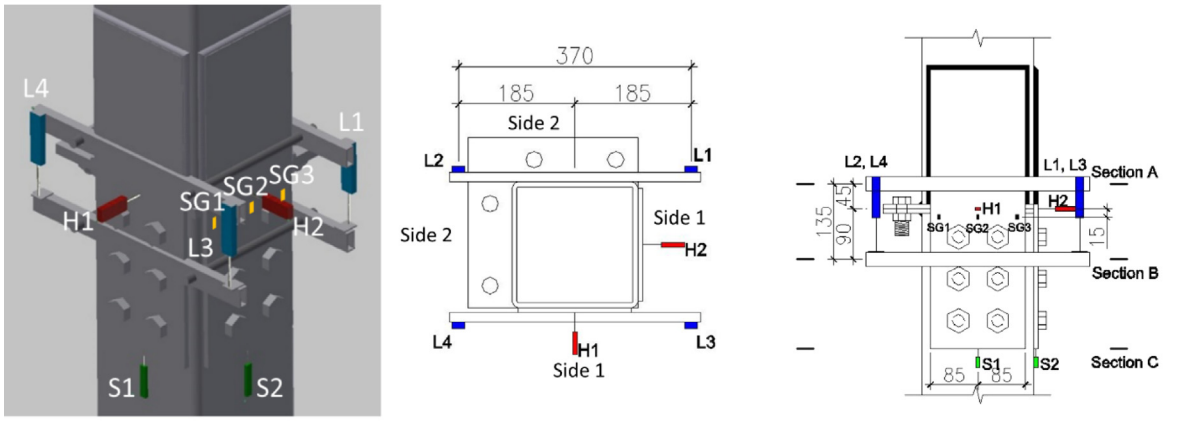

b) Corner column splice.

Appendix C. Schematic drawings for employed components.

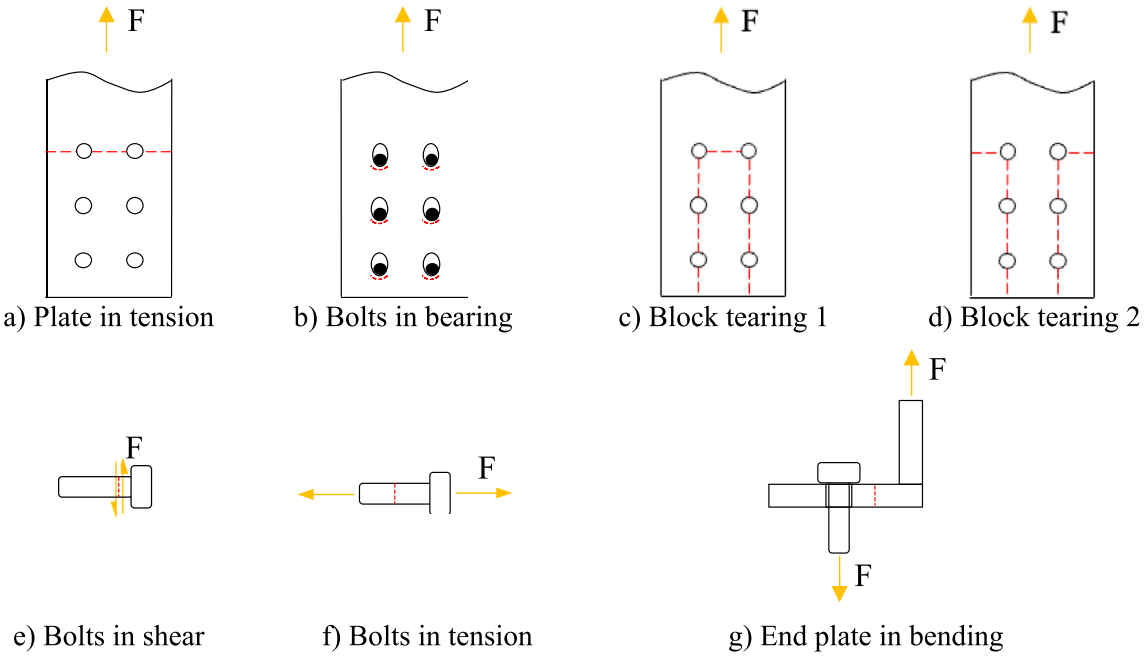

a) Plate in tension b) Bolts in bearing c) Block tearing 1 d) Block tearing 2

e) Bolts in shear f) Bolts in tension g) End plate in bending

References

[1] G.Q. Li, K. Liu, Y.B. Wang, Z. Dai, Moment resistance of blind-bolted SHS column splice joint subjected to eccentric compression, Thin-Walled Struct. 141 (2019) 184–193, http://dx.doi.org/10.1016/j.tws.2019.04.015.

[2] M. Mahmood, W. Tizani, A component model for column face in bending of extended HolloBolt connections, J. Constr. Steel Res. 182 (2021) 106655, http://dx.doi.org/10.1016/j.jcsr.2021.106655.

[3] P. Wang, L. Sun, B. Zhang, X. Yang, F. Liu, Z. Han, Experimental studies on T-stub to hollow section column connection bolted by T-head square-neck one-side bolts under tension, J. Constr. Steel Res. 178 (2021) 106493, http://dx.doi.org/10.1016/j.jcsr.2020.106493.

[4] R. He, X. Shu, Z. Zhang, Experimental study on the tensile performance of high-strength blind-bolted T-stub with endplate tapping, J. Eng. Sci. Technol. Rev. 11 (2018) 109–118, http://dx.doi.org/10.25103/jestr.115.13.

[5] M. D'Antimo, J.F. Demonceau, J.P. Jaspart, M. Latour, G. Rizzano, Experimental and theoretical analysis of shear bolted connections for tubular structures, J. Constr. Steel Res. 138 (2017) 264–282, http://dx.doi.org/10.1016/j.jcsr.2017.07.015.

[6] L. Roquete, M.M. de Oliveira, A.M.C. Sarmanho, E.M. Xavier, V.N. Alves, Behavior and design formulation of steel CHS with sleeve connections, J. Constr. Steel Res. 177 (2021) 106465, http://dx.doi.org/10.1016/j.jcsr.2020.106465.

[7] Z. Chen, J. Liu, Y. Yu, Experimental study on interior connections in modular steel buildings, Eng. Struct. 147 (2017) 625–638, http://dx.doi.org/10.1016/j.engstruct.2017.06.002.

[8] S.N. Sadeghi, A. Heidarpour, X.L. Zhao, R. Al-Mahaidi, A component-based model for innovative prefabricated beam-to-hybrid tubular column connections, Thin-Walled Struct. 132 (2018) 265–275, http://dx.doi.org/10.1016/j.tws.2018.08.021.

[9] prEN 1993-1-8:2021 - Design of steel structures - Part 1-8: Design of joints, 2022.

[10] B. Kato, A. Mukai, Bolted tension flanges joining square hollow section members, J. Constr. Steel Res. 5 (1985) 163–177, http://dx.doi.org/10.1016/0143-974X(85)90001-X.

[11] S. Willibald, Bolted connections for rectangular hollow sections under tensile loading, 2003, p. 221.

[12] F.T. Karlsen, A. Aalberg, Bolted Rhs end-plate joints in axial tension, 2012, pp. 1–12.

[13] J.A. Packer, L. Bruno, P.C. Birkemoe, Limit analysis of bolted RHS flange plate joints, J. Struct. Eng. 115 (1989) 2226–2242, http://dx.doi.org/10.1061/(asce)0733-9445(1989)115:9(2226).

[14] B. Kato, A. Mukai, Bolted tension flanges joining square hollow section members-Supplement: Bolted at two sides of flange, 1985.

[15] S. Jha, D.B. J, Tests on bolted T-stubs with respect to a bolted beam-to-column connection, 1969.

[16] Y. Steige, K. Weynand, Design resistance of end plate splices with hollow sections, Steel Constr. 8 (2015) 187–193, http://dx.doi.org/10.1002/stco.201510023.

[17] K. Weynand, J.-P. Jaspart, J.F. Demonceau, L. Zhang, Component method for tubular joints, 2015.

[18] M. Couchaux, M.D. Aniello, L. Falciano, B. Faggiano, M. Hjiaj, R. Landolfo, Finite element simulations on the tensile resistance of bolted end- plate connections with tubular members, Open Constr. Build. Technol. J. 12 (2018) 177–186, http://dx.doi.org/10.2174/1874836801812010177.

[19] Hilkka. Ronni, Markku. Heinisuo, Test Report, End Plate Joints of Steel Tubes, Biaxial and Weak Axis Bending, (n.d.).

[20] A.T. Wheeler, M.J. Clarke, G.J. Hancock, T.M. Murray, Design model for bolted moment end plate connections joining rectangular hollow sections, J. Struct. Eng. 124 (1998) 164–173, http://dx.doi.org/10.1061/(ASCE)0733-9445(1998)124:2(164).

[21] M. Heinisuo, H. Ronni, H. Perttola, A. Aalto, T. Tiainen, End and base plate joints with corner bolts for rectangular tubular member, J. Constr. Steel Res. 75 (2012) 85–92, http://dx.doi.org/10.1016/j.jcsr.2012.03.013.

[22] C. Ding, Y. Bai, C. Qiu, C. Wan, X.L. Zhao, Steel bolted flanged connections in tension: Effects of stiffener configurations, Thin-Walled Struct. 154 (2020) 106824, http://dx.doi.org/10.1016/j.tws.2020.106824.

[23] S.V. Sendanayake, D.P. Thambiratnam, N.J. Perera, T.H.T. Chan, S. Aghdamy, Enhancing the lateral performance of modular buildings through innovative inter-modular connections, Structures 29 (2021) 167–184, http://dx.doi.org/10.1016/j.istruc.2020.10.047.

[24] C. Qiu, Y. Bai, Z. Cai, Z. Zhang, Cyclic performance of splice connections for hollow section fibre reinforced polymer members, Compos. Struct. 243 (2020) http://dx.doi.org/10.1016/j.compstruct.2020.112222.

[25] F.W. Shi, Y.M. Li, Innovative inner sleeve composite bolted connections for modular steel constructions: Experimental and numerical studies, J. Build. Eng. 64 (2023) http://dx.doi.org/10.1016/j.jobe.2022.105624.

[26] A.W. Lacey, W. Chen, H. Hao, K. Bi, Simplified structural behaviours of post-tensioned inter-module connection for modular buildings, J. Constr. Steel Res. 175 (2020) http://dx.doi.org/10.1016/j.jcsr.2020.106347.

[27] C. Yang, H. Chen, J. Ou, Experimental study on seismic performance of modular steel construction beam-to-beam combined side column joint with blind bolted connection, Thin-Walled Struct. 184 (2023) http://dx.doi.org/10.1016/j.tws.2022.110431.

[28] A.W. Lacey, W. Chen, H. Hao, K. Bi, F.J. Tallowin, Shear behaviour of post-tensioned inter-module connection for modular steel buildings, J. Constr. Steel Res. 162 (2019) http://dx.doi.org/10.1016/j.jcsr.2019.105707.

[29] Metallic materials - Tensile testing - Part 1: Method of test at room temperature (ISO 6892-1:2019), 1, 2019.

[30] ABAQUS, Abaqus Analysis User's Manual, 6.14 version, 2014.

[31] EN 1090-2: Execution of steel structures and aluminium structures - Part 2 2018 Technical requirements for steel structures, (n.d.).

[32] O.S. Bursi, J.P. Jaspart, Benchmarks for finite element modelling of bolted steel connections, J. Constr. Steel Res. 43 (1997) 17–42, http://dx.doi.org/10.1016/S0143-974X(97)00031-X.

[33] O.S. Bursi, J.P. Jaspart, Basic issues in the finite element simulation of extended end plate connections, Comput. Struct. 69 (1998) 361–382, http://dx.doi.org/10.1016/S0045-7949(98)00136-9.

[34] R. Stroetmann, T. Kästner, A. Hälsig, P. Mayr, Influence of the cooling time on the mechanical properties of welded HSS-joints, Steel Constr. 11 (2018) 264–271, http://dx.doi.org/10.1002/stco.201800019.

[35] R. Yan, K. Mela, F. Yang, H. El Bamby, M. Veljkovic, Equivalent material properties of the heat-affected zone in welded cold-formed rectangular hollow section connections, Thin-Walled Struct. (2022).

[36] R. Yan, K. Mela, H. El Bamby, M. Veljkovic, Experimental investigation on the tensile behaviour of welded RHS high strength steel X-joints, Eng. Struct. (2022).